An-Najah University Journal for Research – A
Natural Sciences

Operation matrix method for solving Sediment loss with generalized Caputo-type fractal-fractional derivative

Ibrahem Abdulrasool[1], RUSUL ABDULSALAM[2], M. M. Shalouf[3], A. S. ALJENSH[4], A. M. Shloof[4], Mays Basim[5*]

Type: Full Article. Received: 26th Apr. 2026, Accepted: 30th Jun, 2026

Accepted Manuscript, In Press

Abstract: Sediment loss (SLO) is a critical geological phenomenon characterized by a reduction in mass over time due to the combined effects of controlling variables such as rock competency, weathering, and erosion. This study aims to develop an efficient numerical method for solving SLO fractal-fractional differential equations (SLO-FFDEs) based on shifted Legendre polynomials (SLPs) and to investigate the effects of the fractal, fractional, and erosion parameters on the sediment loss dynamics. The SLO-FFDEs are approximated using the basis vectors of SLPs, and a derivative operational matrix (OM) of SLPs is developed within the framework of the new generalized Caputo fractal-fractional derivative (GCFFD). The proposed method is evaluated for different values of the fractal parameter σ, fractional parameter ϱ, and decaying parameter λ associated with erosion. The numerical results demonstrate that the proposed OM-based framework provides an effective and accurate approach for describing the dynamics of sediment loss under different combinations of fractal and fractional parameters. The results also indicate that variations in the fractal and fractional parameters significantly influence the behavior of the SLO model, while the erosion parameter controls the rate of sediment loss. Therefore, the proposed method provides a flexible computational framework for modeling SLO-FFDEs and can be used to investigate the influence of fractal, fractional, and erosion effects in sediment-loss processes. It is recommended that the proposed framework be further extended to more complex sediment-loss models and validated using experimental or field data.

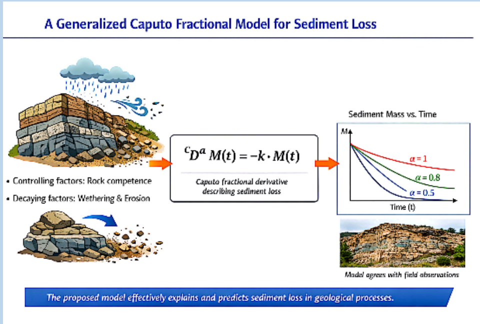

Keywords: Fractal-fractional calculus, environmental sustainability, soil erosion prediction, sustainable land management, climate change, geological processes, memory effects, shifted Legendre polynomials, generalized Caputo derivative.

Introduction

Natural hazards and climatic land erosion play a minor role in SLO [1] and transportation within the sedimentary basin. In mathematical investigations, quantitative analysis [2-5] models are essential to determining the rate of SLO as well as its regulating and decaying elements. According to this theory, a balance exists between the erosion of sedimentary, metamorphic, and igneous rocks, with the total mass of the sediments remaining constant. Another theory is the linear accumulation design, which suggests that the rate of erosion of igneous rocks exceeds the rate of formation of igneous mass. Moreover, sedimentary rocks can be altered to become igneous or metamorphic rocks. Traditional methods for quantifying SLO are quite expensive and require significant labour.

As a result, the use of mathematical modelling to estimate SLO in a sedimentary basin is well supported [2, 6]. Additionally, combining the controlling erosion rates and timescale will reveal a variety of impacts on the rate of SLO.

SLO is heavily reliant on its governing elements, including sediment transport methods, erosion rate, and erosion mechanics. Rainfall has a major role in the movement of SLO from the original rock mass, in addition to acting as an agent of erosion. The rate of precipitation has a significant impact on erosion. Additionally, the effects of rainfall patterns, intensity, and surface runoff on erosion and SLO vary. In a sedimentary basin, SLO is significantly influenced by a variety of sources. By taking into account the topography and erosion elements that contribute to SLO processes throughout a specific time period, the sediment delivery distributed (SEDD) model provides more insight into this process.

In [7], SLO with geomorphological constraints was described using a regression model to explain the SLO concentration in runoff caused by rainfall over a specific time interval. This model appears to be quite helpful in determining SLO per unit time, and the data are exact when compared to the originally observed

1 Department of Accounting Techniques, Administrative Polytechnic College–Baghdad, Middle Technical University, Baghdad, Iraq.
2 Department of Computer Systems Technologies, Administrative Polytechnic College–Baghdad, Middle Technical University, Baghdad, Iraq.
3 Department of Networking, College of Information and Technology, University of Zintan, Al-Zintan, Libya.
4 Department of Mathematics, Faculty of Sciences, University of Zintan, Zintan, Libya.
5 General Directorate of Wasit Education, Ministry of Education, Wasit, Iraq.
* Corresponding author: gs54600@student.upm.edu.my
ORCID iD: https://orcid.org/0000-0003-2061-9583

sediment yield. Recently, [1] provided a detailed quantitative analysis of SLO.

Because of their increased flexibility, generalized fractional operators incorporating the parameters ϱ and ρ have garnered significant attention in fractional calculus. The generalized Caputo derivative [8-11] offers a more comprehensive framework for building fractional mathematical models while preserving the key components of the standard Caputo derivative. Apart from the fractional order, the parameter ρ provides additional control over the solution's behaviour. The operator is very helpful for modelling complicated systems with a variety of dynamic properties because changing this parameter might result in varied solution profiles and graphical patterns.

The fractal derivative, alongside fractional calculus [12], broadens the classical Leibniz derivative to operate within non-integer-dimensional time-space domains. This operator is especially useful for modeling anomalous diffusion in complex and porous media, where standard integer-order models fail to accurately represent transport processes. Unlike classical laws such as Fick's, Darcy's, and Fourier's, the fractal derivative considers the irregular structures and particle interactions inherent in fractal environments. Consequently, it has become an essential tool for studying diffusion and transport phenomena in heterogeneous systems and is applied in various scientific disciplines.

Recently, FFDEs have become increasingly popular due to their unique and adaptable qualities [12]. FFD tools are used to solve non-integer-order derivatives. One significant and practical idea is the GCFFD in fractal-fractional calculus.

In the present paper, we intend to extend the application of OM based on Legendre polynomials to solve SLO fractal-fractional differential equations. It is worthy to mention here that the method based on using the OM of an orthogonal function for solving differential equations is computer-oriented. These definitions are used in our study to solve the considered SLO-FFDE by a numerical technique, namely, the OM of derivative based on SLPS [13-17]. OM methods have become a powerful and widely used tool for the numerical solution of differential, integral, and integro-differential equations, including those of fractional order. The core idea is to represent the unknown solution using appropriate basis functions, such as orthogonal polynomials, and then apply OM to convert differentiation, integration, or fractional operators into matrix operations. This conversion transforms the original problem into a system of algebraic equations, which can be solved efficiently with standard numerical techniques. In recent years, polynomials like Legendre [18,19], Chebyshev, and Genocchi [20-24] have been used to approximate solutions of fractional differential equations (FDEs) by transforming them into algebraic systems using operational matrices. Extensions to fractional orders have shown improved accuracy. Despite progress, few studies address generalized fractional operators, which unify different fractional operators. Exploring these generalized operators is an important ongoing research area.

The popularity of OM methods is due to their ability to reduce computational complexity, achieve high accuracy with relatively few basic functions, and provide a systematic framework for a wide range of mathematical models in science and engineering. Consequently, many OMs based on various polynomial families have been developed and successfully applied to numerous boundary value, initial value, and fractional differential problems. The suggested equations are transformed into an algebraic system of equations using the numerical scheme, which can then be solved using any standard method. The computational approach has many advantages. One of the most important functions is to calculate OM accurately. Finally, to evaluate the accuracy of the suggested method, we consider the results in tables and graphs.

Motivated by previous studies, the fractional SLO model is rewritten within the framework of GCFFD. This study is, to our knowledge, the first investigation into the SLO model in the fractal-fractional-calculus framework. The generalized model is then solved using the OM technique.

This research is organized as follows: In Section 2, we present some meaningful results from the literature on generalized fractional derivatives and fractal-fractional calculus, as well as the basic definition of the shifted Legendre polynomial (SLPS) and OM. Section 3 describes how to solve the SLO fractal-fractional model by extending the FFD of the SLPS-OM with GCFFD. Section 4 presents the algorithm for the solution of SLO-FFDEs. Section 5 provides the paper's results and discussion. Finally, the main conclusions of the study are summarised in Section 6.

Preliminaries

Definition: [25]. The Caputo fractional derivative of order $\varrho > 0$ is defined as:

$$ {}^{C}\wp^{\varrho}_{a+}Z(t) = \frac{1}{\Gamma(\hbar-\varrho)}\int_a^t (t-\tau)^{\hbar-\varrho-1}\ Z^{(\hbar)}(\tau)d\tau, \quad t>a, \qquad (1)$$

where $\hbar - 1 < \varrho \leq \hbar$ and $\hbar \in N$.

Definition: [26]. The generalized Caputo-type fractional derivative (GCFD) of order $\varrho > 0$ is defined as:

$$ {}^{C}\wp^{\varrho,\rho}_{a+}Z(t) = \frac{\rho^{\varrho-\hbar+1}}{\Gamma(\hbar-\varrho)}\int_a^t s^{\rho-1}(t^{\rho} - s^{\rho})^{\hbar-\varrho-1}\left(s^{1-\rho}\frac{d}{ds}\right)^{\hbar} Z(s)\, ds\,, t>a, \qquad (2)$$

where $\rho > 0$, $a \geq 0$, $\hbar - 1 < \varrho < \hbar$, $\hbar = \lceil \varrho \rceil$, and $Z(t) \in C^{\hbar}[a,b]$. Additionally, the GCFD [26, 8] has:

$$ {}^{C}\wp^{\varrho,\sigma}c = 0, \quad \text{c is a constant.} \qquad (3)$$

Besides that, if $\omega - 1 < \varrho < \omega$, $\hbar > \omega - 1$ and $\hbar \notin N$.

$$ {}^{C}\wp^{\varrho,\rho}_{a+}(t^{\rho} - a^{\rho})^{\hbar} = \begin{cases} \rho^{\varrho}\frac{\Gamma(\hbar+1)}{\Gamma(\hbar-\varrho+1)}(t^{\rho}-a^{\rho})^{\hbar-\varrho} & ,\hbar \in \mathbb{N}_0 and\ \hbar \geq \lceil \varrho \rceil . \\ 0 & ,\hbar \in \mathbb{N}_0 and\ \hbar < \lceil \varrho \rceil . \end{cases} \qquad (4)$$

Notably, setting $\rho=1 $ converts the GCFD into the Caputo fractional derivative Eq. (2.1).

Definition: [10] Let be fractal differentiable and continuous of order σ on (a,b), then the GCFFD of $Z(t)$, say ${}^{C}\wp^{\varrho,\rho,\sigma}_{a+}Z(t)$, of order ϱ, σ and ρ is defined as:

$$ {}^{C}\wp^{\varrho,\rho,\sigma}_{a+}Z(t) = \frac{\rho^{\varrho-\hbar+1}}{\Gamma(\hbar-\varrho)}\int_a^t s^{\rho-1}\ (t^{\rho} - s^{\rho})^{\hbar-\varrho-1}\ \left(s^{1-\rho}\frac{d}{ds^{\sigma}}\right)^{\hbar} Z(s)\, ds,\ t>a, \qquad (5)$$

where:

$$\frac{dZ}{dt^{\sigma}} = \lim_{t\to s}\frac{Z(t)-Z(s)}{t^{\sigma}-s^{\sigma}}, \text{ and } 0 < \hbar - 1 < \rho, \varrho \leq \hbar.$$

The formulation in Eq. (6) encompasses the GCFD Eq. (2), which is retrieved by assigning the value $\sigma = 1$.

Definition: [23] The analytic SLPS $\Omega_r(t), t \in [0,1]$, of degree r is given as:

$$\Omega_r(t) = \sum_{\hbar=0}^{r}(-1)^{r+\hbar}\ \frac{(r+\hbar)!\ t^{\hbar}}{(r-\hbar)!\ (\hbar!)^2}, \qquad (6)$$

for example, $\Omega_0(t) = 1$, $\Omega_1(t) = 2t - 1$ and, $\Omega_2(t) = 6t^2 - 6t + 1$, we can show it in Figure 1.

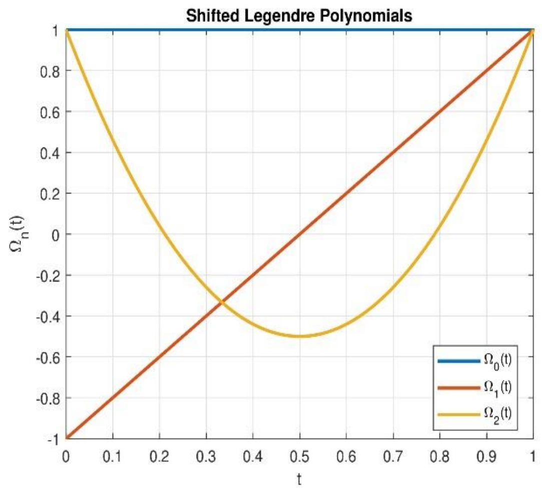

Figure (4): Graphs of the first three Legendre polynomials, $\Omega_0(t), \Omega_1(t)$ and $\Omega_2(t)$.

where $\Omega_r(0) = (-1)^r$ and $\Omega_r(1) = 1$ with the orthogonality condition provided by

$$\int_0^1 \Omega_n(t)\Omega_\omega(t)dt = \begin{cases} \frac{1}{2n+1}, & for\ n = \omega \\ 0 & , for\ n \neq \omega. \end{cases} \quad (7)$$

Let $Z(t) \in \mathcal{L}^2[0,1]$. In terms of the SLPS, we can expand as follows [23]:

$$Z(t) = \sum_{q=0}^{\infty} c_q \Omega_q(t), \quad (8)$$

where:

$$c_q = (2q+1)\int_0^1 Z(t)\ \Omega_q(t)\ dt, \quad q = 1,2,\ldots. \quad (9)$$

If we truncate the preceding series, we get the first $(\omega+1)$-terms of SLPS as follows:

$$Z(t) \simeq \sum_{q=0}^{\omega} c_q \Omega_q(t) = C^T \zeta(t) \quad (10)$$

where C^T and $\zeta(t)$ are vectors defined as

$$C^T = [c_0, c_1, \ldots, c_\omega], \quad \zeta(t) = [\Omega_0(t), \Omega_1(t), \ldots, \Omega_\omega(t)]^T. \quad (11)$$

The first derivative of the shifted Legendre vector $\zeta(t)$ is expressed as

$$\frac{d\zeta(t)}{dt} = \Psi^{(1)}\zeta(t), \quad (12)$$

where $\Psi^{(1)}$ is the OM of order $(\omega+1)$, the elements of which are given by:

$$\Psi^{(1)} = (\varpi_{p,q}) =$$
$$\begin{cases} 2(2q+1), for\ q = p - g, \begin{cases} g = 1,3,\ldots,\omega, if\ \omega\ odd, \\ g = 1,3,\ldots,\omega-1, if\ \omega\ even, \end{cases} \\ 0, \qquad\qquad\qquad otherwise. \end{cases} \quad (13)$$

For the n-th order, we can express it as:

$$\frac{d^n\zeta(t)}{dt^n} = \left(\Psi^{(1)}\right)^{(n)} \zeta(t) \quad , \quad n \in N. \quad (14)$$

OM OF FFDE

This section discusses OM based on SLPS via FFD. (16) The OM based on SLPS was shown in [10] for solving FFDE using OM.

Corollary: [14] Assume that $\varrho, \rho \in (0,1)$ and $\hbar \in N_0 = N \cup \{0\}$ and $\sigma \in \mathbb{R}$. Then we have:

$$^{C}\wp^{\varrho,\sigma,\rho}\ t^{\hbar} = \frac{\sigma^{\varrho}\ \Gamma(\hbar/\sigma+1)}{\rho\ \Gamma(\hbar/\sigma-\varrho+1)}\ t^{\hbar/\sigma-\varrho-\rho+1}. \quad (15)$$

Theorem: [14] Let $\zeta(t)$ be the shifted Legendre vector introduced in Eq.(11) $\varrho > 0$, then

$$\wp^{(\varrho,\sigma,\rho)}\zeta(t) \simeq \Psi^{(\varrho,\sigma,\rho)}\zeta(t), \quad (16)$$

where $\Psi^{(\varrho,\sigma,\rho)}$ is the $(\omega+1)$-order OM of the FFD of the order $\varrho > 0$ and $n-1 < \varrho < n$ in the GCFFD and can be stated as:

$$\Psi^{(\varrho,\sigma,\rho)} = \delta_{(i,j,k)}$$
$$= \begin{pmatrix} 0 & 0 & \cdots & 0 \\ \vdots & \vdots & \cdots & \vdots \\ 0 & 0 & \cdots & 0 \\ \sum_{\hbar=\lceil\varrho\rceil}^{\lceil\varrho\rceil} \Upsilon_{\lceil\varrho\rceil,0,\hbar} & \sum_{\hbar=\lceil\varrho\rceil}^{\lceil\varrho\rceil} \Upsilon_{\lceil\varrho\rceil,1,\hbar} & \cdots & \sum_{\hbar=\lceil\varrho\rceil}^{\lceil\varrho\rceil} \Upsilon_{\lceil\varrho\rceil,\omega,\hbar} \\ \vdots & \vdots & \cdots & \vdots \\ \sum_{\hbar=\lceil\varrho\rceil}^{\rho} \Upsilon_{\rho,0,\hbar} & \sum_{\hbar=\lceil\varrho\rceil}^{\rho} \Upsilon_{\rho,1,\hbar} & \cdots & \sum_{\hbar=\lceil\varrho\rceil}^{\rho} \Upsilon_{\rho,\omega,\hbar} \\ \vdots & \vdots & \cdots & \vdots \\ \sum_{\hbar=\lceil\varrho\rceil}^{\omega} \Upsilon_{\omega,0,\hbar} & \sum_{\hbar=\lceil\varrho\rceil}^{\omega} \Upsilon_{\omega,1,\hbar} & \cdots & \sum_{\hbar=\lceil\varrho\rceil}^{\omega} \Upsilon_{\omega,\omega,\hbar} \end{pmatrix} \quad (17)$$

where $\Upsilon_{p,q,\hbar}$ given by the relation:

$$\Upsilon_{p,q,\hbar} = (2q+1)$$
$$\sum_{l=0}^{q} \frac{\sigma^{\varrho}(-1)^{p+\hbar+q+l}(p+\hbar)!(q+l)!\Gamma\left(\frac{\hbar}{\sigma}+1\right)}{(\hbar!)^2(p-\hbar)!(q-l)!p\Gamma(\frac{\hbar}{\sigma}-\varrho+1)(\frac{\hbar}{\sigma}-\varrho-p+l+2)} \quad (18)$$

for example, $\omega = 2$, $\varrho = 3/2$ and $\rho = 1$

$$(16/\sqrt{\pi})\begin{pmatrix} 0 & 0 & 0 \\ 0 & 0 & 0 \\ 1 & 3/5 & -1/7 \end{pmatrix}$$

Solving the SLO-FFD model

We introduce the applications of SLPS-OM via GCFFD for solving SLO-FFDE [1] in this section. To accomplish this, consider the following model:

$$^{C}\wp^{\varrho,\sigma,\rho}\ Z(t) = -\lambda Z(t), \quad (19)$$

with its initial condition:

$$Z(0) = Z_0. \quad (20)$$

where the $\wp^{\varrho,\sigma,\rho}$ denotes the GCFFD and $(-\lambda)$ is rock competence or strength.

The exact solution in the fractional model [1] is

$$Z(t) = Z_0\ E_{\varrho}(-\lambda t^{\varrho}), \quad (21)$$

Where

$$E_{\varrho}(t) = \sum_{\hbar=0}^{\infty} \frac{t^{\hbar}}{\Gamma(\varrho\hbar+1)}. \quad (22)$$

When $\varrho = \sigma = \rho = 1$, the exact solution is

$$Z(t) = Z_0\ e^{-\lambda t}. \quad (23)$$

The decaying parameter is used as an erosion factor in this study. The suggested model produces the precise answer shown in Eq.(21) for the specific situation $\rho = \sigma = 1$.

First, by SLPS, we approximate $Z(t)$ as follows:

$$Z(t) \simeq \sum_{p=0}^{\omega} c_p\ \Omega_p(t) = C^T\zeta(t), \quad (24)$$

where $C = [c_0, c_1, \ldots, c_\omega]^T$ vector is an unidentified vector. Using Eq. (24), we obtain:

$$\wp^{\varrho,\sigma,\rho}\ Z(t) \simeq C^T\ \wp^{\varrho,\sigma,\rho}\ \zeta(t) \simeq C^T\ \Psi^{(\varrho,\sigma,\rho)}\ \zeta(t), \quad (25)$$

By replacing Eq.(24) in Eq.(19) the residual $R_\omega(t)$ can be represented as follows:

$$R_\omega(t) \simeq \left(C^T\Psi^{(\varrho,\sigma,\rho)} + \lambda C^T\right)\zeta(t). \quad (26)$$

We get $\omega - n$ linear equations by applying:

$$\int_0^1 R_\omega(t)\Omega_q(t)\ dt = 0, \quad q = 0,1,\ldots\omega-1. \quad (27)$$

Substitute Eqs. (24) in Eq.(20) then we have:

$$Z(0) = C^T\ \zeta(0) = Z_0. \quad (28)$$

Eqs. (27) and (28) yield a set of linear equations worth $(\omega+1)$. These linear equations are easily solved for unknown coefficients of the vector C, and then $Z(t)$ can be computed from Eq.(24).

SLOM Algorithm for the Solution of SLO-FFDEs

The complete procedure of the SLOM approach for solving SLO-FFDEs using SLPS in the GCFFD sense is detailed in the following algorithm.

Algorithm 4.1: SLOM Algorithm for SLO-FFDEs.

INPUT ω, ϱ, σ, ρ, initial conditions/boundary conditions.

OUTPUT Approximate solution $Z(t)$.

Step 1 For $i = \lceil\varrho\rceil: \omega$,

For $j = 0: \omega$,

For $k = i: \omega$,

put $\Psi^{\varrho,\sigma,\rho} = \delta_{i,j,k}$, Eq. (17).

Step 2 For $n = 0: \omega$,

put $C^T = [c_0, c_1, \dots, c_\omega]$,

put $\zeta(t) = [\Omega_0(t), \Omega_1(t), \dots, \Omega_\omega(t)]^T$, Eq.(11).

Step 3 $\wp^{\varrho,\sigma,\rho} = C^T \Psi^{\varrho,\sigma,\rho} \zeta(t)$.

Step 4 Approximate $Z(t)$ by SLPS Eq.(10),

$Z(t) = C^T \zeta(t)$.

Step 5 Compute the OM for the given fractal–fractional problem and obtain the resulting algebraic system.

Step 6 Calculate the unknown coefficients

$C^T = [c_0, c_1, \dots, c_\omega]$.

Step 7 Calculate $Z(t) \simeq \sum_{j=0}^{\omega} c_j \Omega_j(t) = C^T \zeta(t)$.

Step 8 STOP

Numerical results and discussion

The research examined SLO parameters, where the mass of rock is represented by $Z(t)$, and the controlling factor is primarily focused on rock strength or competence. In this study, we chose $\omega = 10$, 8 and 15 as the order of OM. For all numerical investigations reported herein, Maple Version 2018 was utilized.

The numerical results of the suggested technique for $Z(t)$ with the parameter values $\varrho = 0.90, 0.99$, $\sigma = 0.97$, $\rho = 1.02$, $\omega = 10$ and $\lambda = 2$ are compared with the exact answer in Figure 2. Throughout the examined time period, it is evident that the numerical solution closely resembles the exact solution.

The excellent precision and dependability of the suggested method in estimating the solution is shown by the overlap between the two curves. Additionally, the small difference between the computed and exact values validates how well the technique captures the system's dynamic nature. These results show that the suggested strategy offers a precise and effective means of resolving the underlying differential model.

In Figure 3, the absolute error associated with $Z(t)$ is evaluated for the case $\varrho = \sigma = \rho = 1$. Table 1 presents the exact and approximate solutions of $Z(t)$ is observed to be very close to the exact solution, along with the corresponding absolute errors for $\varrho = \sigma = \rho = 1$.

Furthermore, a comparison between the exact solution and the outcomes produced by the proposed method for $Z(t)$ is carried out under the parameters $\varrho = 0.98$, $\omega = 10$, $\rho = 1.2$, $\lambda = 5$ and $\sigma = 0.97$.

Meanwhile, Table 2 illustrates the proposed technique results for $Z(t)$ under the parameters $\omega = 10, \varrho = 0.99$, $\rho = 1$, $\lambda = 1.1$ and $\sigma = 1$. Moreover, Table 3 and Figure 4 present the outcomes of the proposed method for $Z(t)$ for different values of the parameters $\omega = 10$, $\varrho = 0.99, 0.98$ and $\rho = 0.98, 1.2$ with different values of λ and σ.

The findings show that when the parameters approach 1, the calculated solution becomes nearly identical to the precise answer.

Figure 5 illustrates a comparison of the results of the approximate and the exact solutions for $Z(t)$ obtained using the proposed method with $\varrho = 0.92$, $\rho = 0.99$, $\omega = 10$, $\lambda = 5$ and $\sigma = 0.97$.

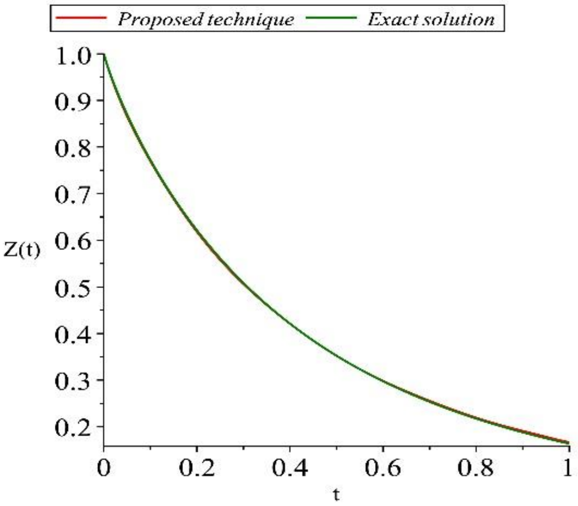

(a)

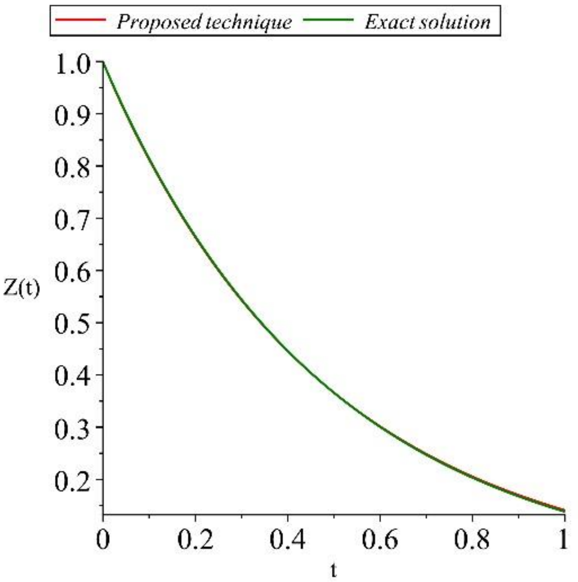

(b)

Figure (2): (a) Comparison of the exact and proposed techniques for $Z(t)$ for $\varrho = 0.90$, $\sigma = 0.97$, $\rho = 1.02$ and $\lambda = 2$. **(b)** Comparison of the exact and proposed techniques for $Z(t)$ for $\varrho = 0.99$, $\sigma = 0.97$, $\rho = 1.02$ and $\lambda = 2$.

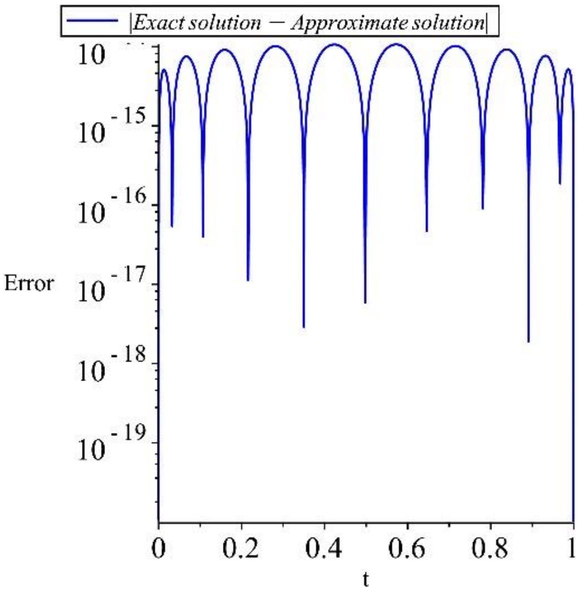

(a)

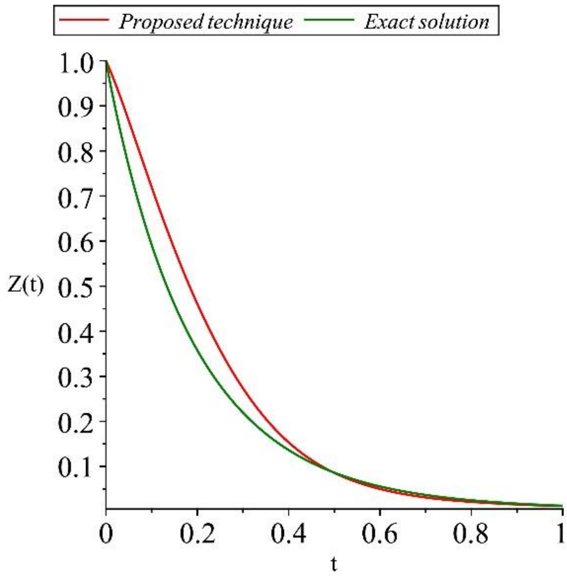

(b)

Figure 3: (a) Comparison of the exact and proposed techniques for $Z(t)$ for $\varrho = 0.90$, $\sigma = 0.97$, $\rho = 1.02$, and $\lambda = 2$. **(b)** Comparison of the exact and proposed techniques for $Z(t)$ for $\varrho = 0.99$, $\sigma = 0.97$, $\rho = 1.02$ and $\lambda = 2$.

Table (1): The proposed technique of $Z(t)$ for where $\omega = 10$, $\varrho = 1$, $\rho = 1$ and $\sigma = 1$.

t	The exact solution	The proposed technique $Z(t)$
0.0	1.0000000000	0.9999999999
0.1	0.9048374180	0.9048374180
0.2	0.8187307531	0.8187307531
0.3	0.7408182207	0.7408182206
0.4	0.6703200460	0.6703200460
0.5	0.6065306597	0.6065306597
0.6	0.5488116361	0.5488116360
0.7	0.4965853038	0.4965853038
0.8	0.4493289641	0.4493289641
0.9	0.4065696597	0.4065696597
1.0	0.3678794412	0.3678794412

Table (2): The proposed technique of $Z(t)$ for where $\omega = 10$, $\varrho = 0.99$, $\rho = 1$, $\lambda = 1.1$ and $\sigma = 1$.

t	The exact solution	The proposed technique $Z(t)$
0.0	1.0000000000	1.0000000000
0.1	0.8931772890	0.8931987007
0.2	0.7991177029	0.7991044301
0.3	0.7154776591	0.7154701506
0.4	0.6409249837	0.6409477809
0.5	0.5743876507	0.5743731357
0.6	0.5149540364	0.5149465794
0.7	0.4618328062	0.4618507800
0.8	0.4143301636	0.4143174220
0.9	0.3718343936	0.3718419450
1.0	0.3338042478	0.3338043900

Table (3): The proposed technique of $Z(t)$ for $\omega = 10$, $\varrho = 0.99$ and $\rho = 0.98$.

t	$\lambda = 0.5, \sigma = 1$	$\lambda = 1.5, \sigma = 0.98$	$\lambda = 0.99, \sigma = 1$
0.0	0.9999999998	0.9999999996	1.0000000000
0.1	0.9467458062	0.8428640144	0.8974879944
0.2	0.8983406470	0.7189024262	0.8092163458
0.3	0.8532198757	0.6162984840	0.7310932980
0.4	0.8108507557	0.5300856800	0.6613587679
0.5	0.7707945127	0.4563901061	0.5985859777
0.6	0.7330158219	0.3939076994	0.5422563275
0.7	0.6972941459	0.3405986790	0.4915438530
0.8	0.6633652750	0.2943983600	0.4455957360
0.9	0.6312781420	0.2551031800	0.4042418800
1.0	0.6007907900	0.2210335000	0.3667545400

The comparison of the absolute errors in $Z(t)$ between the suggested technique and the method of [23] for $\omega = 8$, $\varrho = 0.85$ and $\sigma = 1$, and artificial neural networks (ANNs) technique [27] for n=5, learning rate and the momentum term are 0.1 and 0.01, respectively, are shown in Table 4. The numerical results support the suggested strategy's improved accuracy and computational efficiency, showing that it consistently yields lower absolute errors. Table 5 presents a comparison of the results for $Z(t)$ obtained using the proposed method with $\omega = 15$, $\varrho = 0.98$ and $\sigma = 0.99$, for $\lambda = 1$ and $\lambda = 5$.

Table (4): Comparison of the absolute errors in $Z(t)$ obtained using the present method and the existing approaches reported in [23, 27] for $\omega = 8$, $\varrho = 0.85$ and $\sigma = 1$.

t	Absolute error of proposed technique	Absolute error of method in [23]	Absolute error of method in [27]
0.1	8.0×10^{-5}	8.0×10^{-4}	1.8×10^{-3}
0.2	1.3×10^{-4}	1.2×10^{-3}	3.1×10^{-3}
0.3	6.6×10^{-5}	6.6×10^{-4}	3.7×10^{-3}
0.4	8.0×10^{-5}	8.0×10^{-4}	3.7×10^{-3}
0.5	7.5×10^{-5}	7.5×10^{-4}	3.2×10^{-3}
0.6	5.9×10^{-5}	5.9×10^{-4}	2.2×10^{-3}
0.7	7.6×10^{-5}	7.6×10^{-4}	9.1×10^{-4}
0.8	1.8×10^{-5}	1.8×10^{-4}	4.4×10^{-4}
0.9	6.2×10^{-5}	6.2×10^{-4}	1.6×10^{-3}
1.0	1.5×10^{-5}	1.5×10^{-4}	2.1×10^{-3}

The comparison of the absolute errors in $Z(t)$ between the suggested technique and the method of [23] for $\omega = 8$, $\varrho = 0.85$ and $\sigma = 1$, and the artificial neural networks (ANNs) technique [27] for n=5, with learning rate and the momentum term set to 0.1 and 0.01, respectively, is shown in Table 4. The numerical results support the suggested strategy's improved accuracy and computational efficiency, as it consistently yields lower absolute errors. Table 5 presents a comparison of the results for $Z(t)$ obtained using the proposed method with $\omega = 15$, $\varrho = 0.98$ and $\sigma = 0.99$, for $\lambda = 1$ and $\lambda = 5$.

Table (5): Comparison of the present method of $Z(t)$ obtained for $\omega = 15$, $\varrho = 0.98$ and $\sigma = 0.99$.

t	$\lambda = 1$	$\lambda = 5$
0.1	0.8998976697	0.5916213310
0.3	0.7342794088	0.2191675900
0.5	0.6014790666	0.0861562090
0.7	0.4940108620	0.0366911320
0.9	0.4066612648	0.0174978600

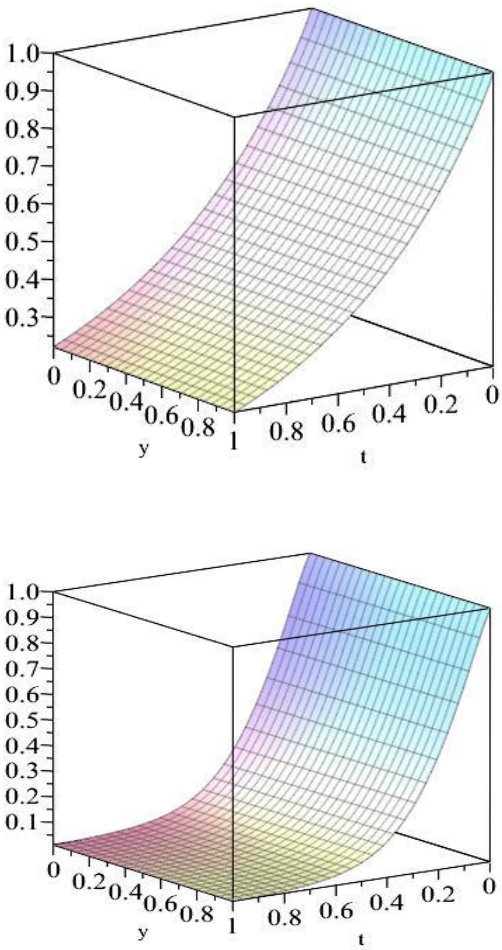

Figure (4): (a) $Z(t)$ for $\varrho = 0.98$, $\rho = 0.98$, $\lambda = 1.5$ and $\sigma = 0.98$. **(b)** $Z(t)$ for $\varrho = 0.99$, $\rho = 1.2$, $\lambda = 5$ and $\sigma = 0.97$.

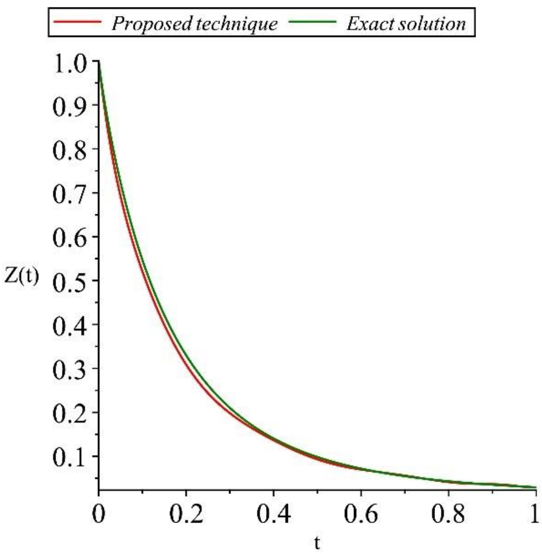

Figure (5): Comparison between the exact and proposed technique of $Z(t)$ for $\varrho = 0.92$, $\rho = 0.99$, $\omega = 10$, $\lambda = 5$ and $\sigma = 0.97$.

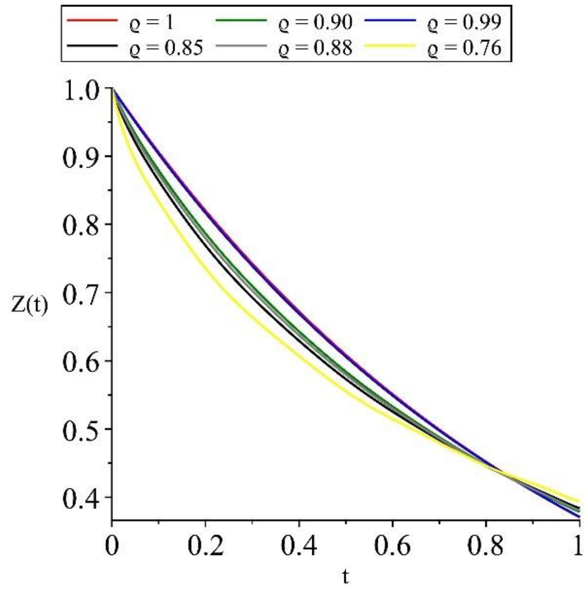

Figure (6): The proposed technique with $\rho = 1.01$, $\sigma = 0.99$ and different values of ϱ.

Figures 6, 7, 8, and 9 present a comparison of the results for $Z(t)$ obtained using the proposed method for different values of ϱ, ρ, σ and λ. The results indicate that the solution is sensitive to the parameter variations. In particular, when ϱ, ρ, σ and λ are close to 1, the approximate solution converges closely to the exact solution.

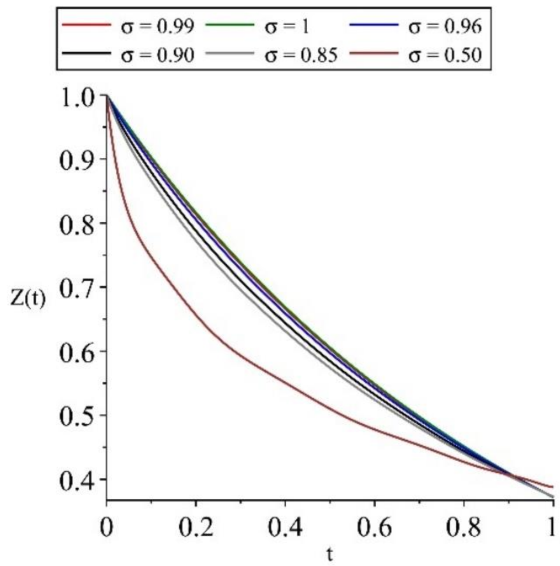

Figure (7): The proposed technique with $\varrho = 0.98$, $\rho = 1.01$ and different values of σ.

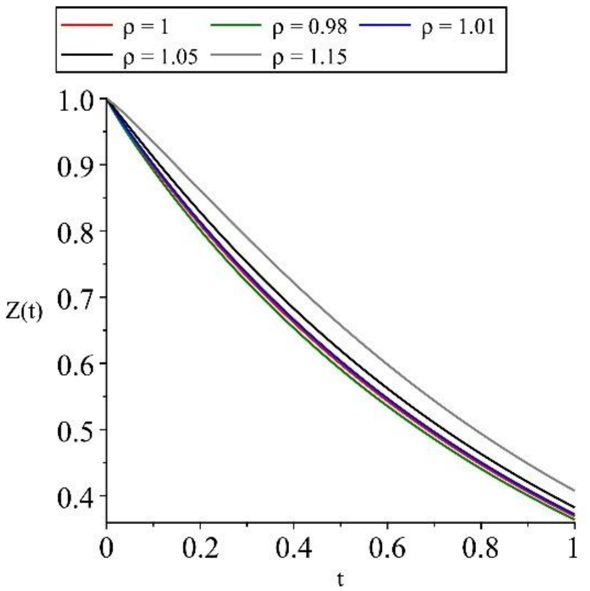

Figure (8): $Z(t)$ for $\varrho = 0.98$, $\lambda = 1$ and $\sigma = 0.99$ with different values of ρ.

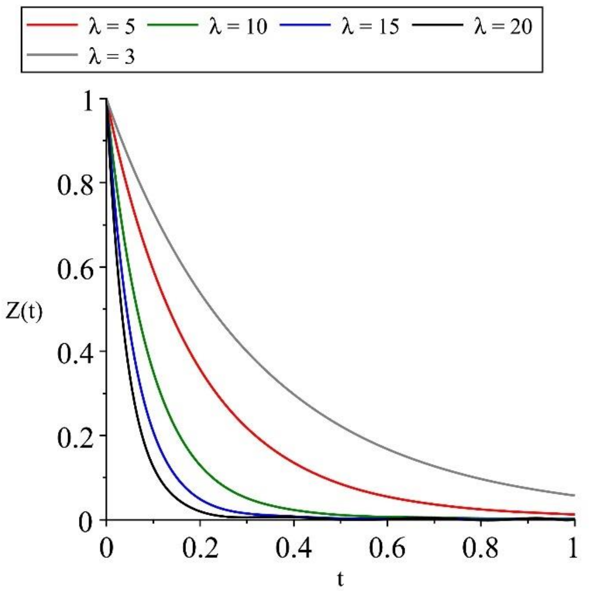

Figure (9): The proposed technique with $\varrho = 0.98,\ \sigma = 0.99,\ \rho = 1.01$ with different values of λ.

Mass reduction is directly correlated with time. In contrast, $\boldsymbol{\lambda}$ is the decaying parameter. In this instance, $\boldsymbol{\lambda}$ is assigned to erosion or weathering. The extent of erosion has a negative impact on mass loss per unit time. The extent of weathering of rocks reduces the initial mass significantly per unit time.

The comparison of the fractional model's approximate and exact solutions is shown in Figures 2 and 3 when $\boldsymbol{\lambda = 2}$ and $\boldsymbol{\lambda = 5}$ for different values of $\boldsymbol{\varrho}$, $\boldsymbol{\rho}$ and $\boldsymbol{\sigma}$.

Tables 3 and 4 show the approximate solution for different values of $\boldsymbol{\lambda}$ and $\boldsymbol{\sigma}$. While Figures 6, 7, 8, and 9 depict the effect of varying $\boldsymbol{\varrho}$ and $\boldsymbol{\rho}$, $\boldsymbol{\sigma}$ and $\boldsymbol{\lambda}$, these figures show that increasing $\boldsymbol{\varrho}$ and $\boldsymbol{\rho}$ yields a good solution.

In this study, erosion values range from 1 to 20, with 3 being the least severe and 20 the most severe. Erosion will be exacerbated by changes in the rate of precipitation and temperature. The decaying parameter beta will be determined by the agents of erosion: wind, water, and organisms. The decaying parameter's value is also affected by climatic conditions and the intensity of erosion.

As a result, the decay factor is the primary determinant of mass reduction per unit time (e.g., weathering or erosion). Figure 9 shows that $\boldsymbol{Z(t)}$ decreases with increasing time and a decaying parameter $\boldsymbol{\lambda}$.

Figure (10): The recent rock exposure brought on by the Pan Borneo highway infrastructure expansion. The time is seen as being close to zero. There is no obvious indication of sediment loss or reduction, and even the rocks with lower values of the regulating factor (shales) are undamaged. The field photo was taken at the Kawang road section of SW Sabah, Malaysia, during the initial stage of geological research. [1,28,29].

Figure (11): Time goes past, and we can witness sediment loss. The second phase of the geological field at the same site depicts the influence of time on the genuine outcrop. Sediments with poor regulating factors (incompetent shales) lose bulk fast compared to their initial mass. This rock fragment clearly demonstrates how mass decreases over time. The field shot was captured at the Kawang road section of SW Sabah, Malaysia, during the second field visit [1].

Figure (12): The impact of a controlling factor on the initial mass loss of sediment. The field photo was taken during the second field visit at the Kawang road sector of SW Sabah, Malaysia. These shales are easily lost over time due to a low controlling factor, whereas the sandstone units remain intact, and no sediment loss occurs for rocks with a high controlling factor. Keeping the time constant, the influence of sediment loss is only visible on the mass with a small controlling factor. The image was shot from the University Prima Condo road portion in Kota Kinabalu, Sabah, Malaysia [1].

Figure (13): The lithologies with low controlling factors will deteriorate as time values increase, and the rocks with strong controlling factors will also begin to disintegrate. In the image, the author highlighted the area formed by shale weathering and erosion, which is considered an ineffective rock with few controllable parameters.

Additionally, the sand units that covered the eroded shale weathered or decomposed into tiny blocks. This indicates that, regardless of the controlling factor, both lithologies experience a distinct reduction in initial mass as time increases. The field photo was taken at Telipok, NW Sabah, Malaysia, close to the University Utama outcrop.

Figure (14): Shows how time affects a highly controlled parameter. Competent lithology (sandstone units) with high regulating factors weathers or erodes over time. Over a longer period, the decrease in sediment levels will have a significant impact on the rock, particularly where controlling factors are strong. Sediment loss occurs over longer time durations, despite the presence of strong controlling factors. The field photo was captured at Benoni Quarry, located in Sabah, Malaysia [1].

This research employs mathematical modelling to describe the relationship between time and sediment loss. The results reveal that sediment bulk reduces gradually over time due to continuous geological processes. The rate of this reduction is determined by a decay parameter that represents erosion intensity. Higher decay values result in rapid mass loss, suggesting weaker materials, whereas lower values correspond to greater resistance and slower erosion. Thus, sediment loss is dependent on both time and the decay parameter, with their interplay defining the total reduction trend. The reduction in mass is primarily dependent on time. However, it is also strongly influenced by the decay parameter $\boldsymbol{\lambda}$, which in this context represents weathering or erosion. The intensity of erosion has a negative impact on the rate of mass loss per unit time. In particular, higher levels of erosion and weathering lead to a more pronounced decrease in the initial mass over time. In this study, the erosion parameter is varied within the range 3 to 20 (see Figure 9), where the value 3 corresponds to the lowest erosion intensity, and 20 represents the highest level considered. Changes in precipitation and temperature further enhance erosional processes. The magnitude and variability of the decay parameter, which represents weathering and erosion processes, differ across geographical regions. In this work, the decay parameter is interpreted as an erosion factor. Its value, denoted by $\boldsymbol{\lambda}$, is governed by erosional agents such as wind, water, and biological activity. Moreover, climatic conditions and the overall intensity of erosion significantly affect this parameter.

Hence, the rate of mass reduction per unit time is mainly controlled by the decay factor associated with weathering and erosion processes. As illustrated in the figure, $\boldsymbol{Z}(\boldsymbol{t})$ decreases as both time and the decay parameter increase.

Figures 10, 11, 12, and Figure 14 show that sediment loss increases with weathering time and the decay parameter. Shale units, characterized by lower controlling factors, undergo faster erosion and contribute more sediment loss than sandstone units. Although sandstone is initially more resistant, prolonged exposure eventually leads to its weathering and disintegration. Overall, time and lithological resistance are the main factors controlling sediment loss.

Conclusion

The purpose of this paper is to investigate the application of FFDE to a geoscientific phenomenon in the sense of GCFFDE. A numerical solution was obtained through the OM technique. The results are graphed and discussed in detail for various values of $\boldsymbol{\varrho}, \boldsymbol{\rho}, \boldsymbol{\sigma}$ and $\boldsymbol{\lambda}$. Changing the values of these parameters allows us to align the mathematical model with geological activity. The fractal parameter can take into consideration the inherent variety of geological surfaces when predicting sediment loss and erosion. In contrast to a homogeneous layer, a sediment layer with a heterogeneous composition and irregular texture may react differently to weathering and erosion processes. As a result, by adding the fractal element, the mathematical model may more accurately describe sediment processes and represent the spatial complexity of geological materials. In general, the fractal parameter is a mathematical signal of structural complexity and irregularity rather than a direct representation of a physical quantity like density or velocity. In situations when traditional models based on uniform assumptions might not be able to adequately describe the observed behavior, it allows fractal-fractional models to depict geological systems.

The numerical results were further supported through graphical analysis and tables. The findings indicate that lithological properties play a crucial role in governing SLO behavior. Incompetent rocks, such as shale, were found to deteriorate more rapidly than competent lithologies, particularly under stronger erosional conditions. While the influence of the decay parameter is more evident in weaker rock units, prolonged exposure to weathering processes ultimately leads to the degradation of both competent and incompetent formations. Furthermore, varying the fractal-fractional-order parameter generated different solution patterns, demonstrating the capability of the fractal-fractional model to capture memory and hereditary effects that are absent in classical integer-order formulations. The proposed framework confirms the effectiveness of fractal-fractional calculus in representing complex geological phenomena and provides a more realistic description of SLO dynamics. We observed that the shales decay quickly due to time variations; two very different competent and incompetent lithologies decay over significant time values. Nevertheless, in the case of incompetent rocks, the decay process is significantly more effective. To the best of our knowledge, the application of this particular fractal-fractional approach to SLO modelling has not been previously reported. Therefore, the present work offers a useful foundation for future studies in geoscience modeling.

Disclosure Statement

- **Ethics approval and consent to participate:** Not applicable.
- **Consent for publication:** Not applicable.
- **Availability of data and materials:** Not applicable.
- **Author's contribution:** All authors made equal contributions to the conceptualization, methodology, formal analysis, validation, writing of the original draft, review, and editing of the manuscript. All authors have read and approved the final manuscript.

- **Funding:** Not applicable.

- **Conflicts of interest:** The authors declare that there is no conflict of interest regarding the publication of this article.
- **Research Source:** This manuscript is an independent research study and is not derived from any master's thesis or doctoral dissertation.

- **Acknowledgements:** The authors would like to thank the reviewers for their valuable comments and constructive suggestions.

Open Access

References

1] Al-Sudani NA, Al-Nuh IAH. Investigation of a new coupled system of fractional differential equations in frame of Hilfer-Hadamard. Nonlinear Funct Anal Appl. 2024;29(2):501-515. doi:10.22771/nfaa.2024.29.02.11.

2] Atangana A. Fractal-fractional differentiation and integration: connecting fractal calculus and fractional calculus to predict complex system. Chaos Solit Fractals. 2017;102:396-406. doi:10.1016/j.chaos.2017.04.027.

3] Basim M, Senu N, Ahmadian A, Ibrahim ZB, Salahshour S. A robust operational matrix of nonsingular derivative to solve fractional variable-order differential equations. Fractals. 2022;30(1):2240041. doi:10.1142/S0218348X22400412.

4] Basim M, Senu N, Ahmadian A, Ibrahim ZB, Salahshour S. Solving fractional variable-order differential equations of the non-singular derivative using Jacobi operational matrix. J Niger Soc Phys Sci. 2023;1221:1221. doi:10.46481/jnsps.2023.1221.

5] Jamil M, Rahman AHA, Siddiqui NA, Ahmed N. Deep marine Paleogene sedimentary sequence of West Sabah: contemporary opinions and ambiguities. Warta Geologi. 2019;45(3):198-200.

6] Jamil M, Rahman AHA, Siddiqui NA, Ibrahim NA, Ahmed N. A contemporary review of sedimentological and stratigraphic framework of the Late Paleogene deep marine sedimentary successions of West Sabah, North-West Borneo. Bull Geol Soc Malaysia. 2020;69:53-65. doi:10.7186/bgsm69202005.

7] Jarad F, Abdeljawad T, Baleanu D. On the generalized fractional derivatives and their Caputo modification. J Nonlinear Sci Appl. 2017;10(5):2607-2619. doi:10.22436/jnsa.010.05.27.

8] Nieto JJ, Rodríguez López R, editors. Fractional differential equations: theory, methods and applications. Basel: MDPI; 2019. doi:10.3390/books978-3-03921-733-5.

9] Odibat Z, Baleanu D. Numerical simulation of initial value problems with generalized Caputo-type fractional derivatives. Appl Numer Math. 2020;156:94-105. doi:10.1016/j.apnum.2020.04.015.

10] Saadatmandi A, Dehghan M. A new operational matrix for solving fractional-order differential equations. Comput Math Appl. 2010;59(3):1326-1336. doi:10.1016/j.camwa.2009.07.006.

11] Sarangi A, Bhattacharya AK. Comparison of artificial neural network and regression models for sediment loss prediction from Banha watershed in India. Agric Water Manag. 2005;78(3):195-208. doi:10.1016/j.agwat.2005.02.001.

12] Sheikh NA, Jamil M, Ling Chuan Ching D, Khan I, Usman M, Nisar KS. A generalized model for quantitative analysis of sediments loss: a Caputo time fractional model. J King Saud Univ Sci. 2021;33(1):101179. doi:10.1016/j.jksus.2020.09.006.

13] Shloof AM, Senu N, Ahmadian A, Nik Long NMA, Salahshour S. Solving fractal-fractional differential equations using operational matrix of derivatives via Hilfer fractal-fractional derivative sense. Appl Numer Math. 2022;178:386-403. doi:10.1016/j.apnum.2022.02.006.

14] Shloof AM, Senu N, Ahmadian A, Nouh MI, Salahshour S. A novel fractal-fractional analysis of the stellar helium burning network using extended operational matrix method. Phys Scr. 2023;98(3):034004. doi:10.1088/1402-4896/acba5d.

15] Shloof AM, Senu N, Ahmadian A, Pakdaman M, Salahshour S. A new iterative technique for solving fractal-fractional differential equations based on artificial neural network in the new generalized Caputo sense. Eng Comput. 2023;39(1):505-515. doi:10.1007/s00366-022-01607-8.

16] Shloof AM, Ahmadian A, Senu N, Salahshour S, Ibrahim SNI, Pakdaman M. A highly accurate artificial neural networks scheme for solving higher multi-order fractal fractional differential equations based on generalized Caputo derivative. Int J Numer Methods Eng. 2023;124(19):4371-4404. doi:10.1002/nme.7312.

17] Shloof AM, Senu N, Ahmadian A, Salahshour S. An efficient operation matrix method for solving fractal-fractional differential equations with generalized Caputo-type fractional-fractal derivative. Math Comput Simul. 2021;188:415-435. doi:10.1016/j.matcom.2021.04.019.